District cooling substation design and control to achieve high return temperatures

N.B. When citing this work, cite the original published paper.

(article starts on next page)

District cooling substation design and control to achieve high return temperatures

Maria Jangsten [a, *], Torbjörn Lindholm [a], Jan-Olof Dalenbäck [a]

[a] *Division of Building Services Engineering, Department of Architecture and Civil Engineering, Chalmers University of Technology, SE-412 96, Gothenburg, Sweden*

ARTICLE INFO

ABSTRACT

Low return temperatures are a prevailing issue in district cooling systems negatively affecting operating costs and energy efficiency. In this study, three aspects of district cooling substation design and control were investigated with the aim to increase the return temperatures: 1) secondary supply temperature setpoint, 2) primary flow rate and 3) the flow rate relation between the primary and secondary flows. Two different control strategies limiting the secondary setpoint and the primary flow were tested in four buildings supplied by district cooling. Also, the secondary flow was measured along with an NTU analysis and predictions with a heat balance and a support vector regression model. The results showed the control strategies successfully increased the primary return temperature with 0.6−1.6 °C and eliminated flow in the saturation zone. The primary and secondary flows were shown to be unbalanced in fourteen of sixteen substations causing a low heat exchanger temperature effectiveness. The preferred method for predicting the secondary flow was support vector regression. The novelties of this paper are the conducted field tests and measurements with associated analyses, contributing with knowledge about the actual operation of district cooling substations and outcomes when implementing improvement measures to increase the primary return temperature.

© 2022 The Author(s). Published by Elsevier Ltd. This is an open access article under the CC BY license (http://creativecommons.org/licenses/by/4.0/).

1. Introduction

District cooling (DC) is a promising technology to meet an increasing global cooling demand [1]. However, issues such as the "low delta-T syndrome", resulting in low return temperatures, continue to cause system inefficiencies and increased costs [2]. The low delta-T syndrome has been researched since the 1980s, but primarily in district cooling systems without heat exchangers separating the customers' chilled water (CHW) system and the distribution system [3]. In district heating (DH) systems, the issue of low delta-T also prevails only the problem is the opposite, with *high* return temperature being a problem. Numerous previous studies have investigated this problem under the research domain "fault detection and diagnosis" in DH substations [4,5]. Although DC and DH share many similarities, DC systems can be distinguished from DH systems by the significantly smaller delta-T

between the supply and return water, 10 °C instead of around 40 °C [6]. Moreover, the building systems on the secondary side of the DC system are different than those supplied by DH systems. The DC substation is also designed and controlled differently than DH substations. Therefore, research outcomes on DH systems may not be directly applicable in DC systems whereby DC systems should be examined separately. Based on previous initial investigations on potential issues causing low delta-Ts of the heat exchanger (HX) in DC substations [3,7], this paper will focus on the control of the secondary supply temperature and the primary and secondary flow rates with the aim to increase the primary return temperature.

1.1. Literature review

The literature review is divided into two sections. The first section focuses on control strategies of the secondary supply temperature and the second section on the primary and secondary flow rates in the HX.

1.1.1. Secondary supply temperature
For DH systems, several previous studies have been conducted

* Corresponding author.
E-mail addresses: maria.jangsten@chalmers.se (M. Jangsten), torbjorn.lindholm@chalmers.se (T. Lindholm), jan-olof.dalenback@chalmers.se (J.-O. Dalenbäck).

Nomenclature

$\dot{Q}$	Cooling power [kW]
$\dot{V}$	Volumetric flow rate [m³/h]
t	Temperature [°C]
Δt	Temperature difference [°C]
$c_{p,w}$	Specific heat capacity of water [kJ/(kg·°C)]
b	Coefficient determining the position of the separating hyperplane
E	Expected value
X	Random variable
y	Data to be transformed

Greek letters

ρ_w	Density of water [kg/m³]
α	Coefficients of support vectors
μ	Mean
σ	Standard deviation
λ	Power transformation
γ	Width parameter of Kernel function

Subscripts

DC	District cooling, substation primary side
DC, supply	Supply stream to heat exchanger: inlet cold side heat exchanger
DC, supply, prod	Supply from DC production plant to DC system
DC, return	Return stream from heat exchanger: outlet cold side heat exchanger
CHW	Chilled water, substation secondary side
CHW, supply	Supply stream to building: outlet warm side heat exchanger
CHW, return	Return stream from building: inlet warm side heat exchanger
out	Outdoor

Abbreviations

AHU	Air Handling Unit
CHW	Chilled Water
DC	District Cooling
DH	District Heating
HX	Heat Exchanger
SCADA	Supervisory Control and Data Acquisition
SVR	Support Vector Regression

to optimize the substation control and the secondary space heating system to increase delta-T. For example, Ljunggren et al. [8] varied the secondary flow and supply temperature with the heat load to achieve an optimal primary return temperature. Lauenburg and Wollerstrand [9] extended this control method to adapt to changes of the primary supply temperature. Gustafsson et al. [10] simulated the control method in Ref. [8] for a single-family home and experimentally verified the method to control the secondary system in an actual DH substation [11]. Oevelen et al. [12] developed a steady-state substation model to investigate optimized control heating curves based on the secondary supply temperature and flow rate to minimize the primary return temperature. The investigated secondary systems in studies [8–12] are all radiator systems. However, the end terminals in building CHW systems supplied by DC usually are combinations of cooling coils in air handling units (AHUs), fan coil units and chilled beams [3,13]. In some secondary systems supplied by DC the supply temperature is controlled with outdoor temperature compensated curves [13], similar to the traditional control of space heating systems supplied by DH [8]. Therefore, based on research done to optimize DH supplied secondary supply temperatures to decrease the primary return temperature, there is a potential of optimizing the supply temperatures in building systems supplied by DC, to increase the primary return temperature.

Another finding from Ref. [10] is the control of space heating systems with traditional outdoor temperature compensated curves works best when the primary supply temperature of the DH system increases when the outdoor temperature drops. This is typical for DH systems [6], but for DC systems the supply temperature is typically constant throughout the year, or with a few different temperature levels for different outdoor temperatures [14]. To maximize the use of free cooling sources [13], some Swedish DC systems are changing to outdoor temperature dependent supply temperatures [15]. It is therefore crucial the buildings' secondary supply temperatures follow the primary supply temperature. This can be ensured by a control strategy maintaining a sufficient temperature approach between the supply streams of the heat exchanger. This is recommended by both national and local Swedish design guidelines of the DC substation [14,15] and was

suggested in Ref. [3] as a potential improvement to low delta-Ts in DC substations. It was also highlighted by Gao et al. in Refs. [7,16], where a low delta-T occurred due to the setpoint on the secondary side being too low in relation to the temperature on the primary side. A similar control strategy was tested for DH substations as demand side management for peak shaving [17]. However, to the authors knowledge, no previous studies have investigated the impact of such a control strategy in Swedish DC systems and the implementation of this control strategy among building owners is unknown.

1.1.2. Primary and secondary flows

A previously established issue with the primary flow in the DC substation causing a low delta-T is the flow in the saturation zone [3]. The saturation zone occurs when the cooling load has reached its peak and become saturated [18]. If flow in the saturation zone occurs in several substations simultaneously, it could potentially cause a strain on the entire DC system. A potential solution is a flow limiting control strategy, restricting the flow on the primary side and preventing flow in the saturation zone [3]. A flow limiter has also previously been suggested as a dynamic load response [6]. However, to the authors knowledge, no studies have evaluated the practical implications of a flow limiting control strategy in a DC substation and what effects it could have on the entire DC system.

Mass flow control of the DH substation was investigated by Kuosa et al. [19] and Laajalehto et al. [20]. The HX was selected for equal heat capacity flow rates on both sides and the mass flow control resulted in a high NTU value of 9.15, an HX effectiveness of 0.9 and a reduced primary return temperature with 2.1 °C compared to traditional control. Iturralde et al. [21] found mass flow control facilitated equal flow rates on both sides of the HX and improved the heat transfer. Gao et al. [7,16] showed the HX flow rates on the secondary and primary sides became unbalanced when the secondary supply temperature setpoint was too low in relation to the primary temperature. These previous studies stress the importance of equal flow rates of the HX. For symmetrical HXs with the same fluid on both sides, the highest effectiveness is achieved when both streams have equal flow rates [9,22,23]. Potential unbalances of the primary and secondary flows may therefore be an

underlying reason to inefficiencies, such as operation with low NTU and temperature effectiveness. However, there is normally no permanent flow measurement equipment installed on the secondary side since this may be economically unjustified. The actual secondary flows are consequently unknown along with the relation between the primary and secondary flows.

In previous simulations and experiments [19−21,24], steady state operation of the HX has been assumed or awaited. In steady state, the flow rate on the secondary side can be calculated based on the simple heat balance, using the primary flow rate and the HX's four inlet and outlet temperatures [8,25]. However, HX operation during transient condition becomes more complex. Gao et al. [26] handled the transient conditions in an HX model by adding a temperature after the introduction of dynamic effects for data generated by simulations. Al-Dawery et al. [27] investigated the transient response of a plate frame HX and developed a general dynamic model. The model was represented by a first order lag plus deadtime, meaning the system is highly non-linear. An example of a highly non-linear subsystem in buildings supplied by DC is the CHW system serving the cooling coils in AHUs. To predict the water flow rate for this non-linear system, Gao et al. [28] used support vector regression (SVR). SVR is a machine learning algorithm based on empirical risk minimization from statistical learning theory [29]. Zhao et al. [30] employed SVR to develop performance index models for three subsystems of a building CHW system. SVR has also been used to predict heat loads in DH systems [31] along with heating and cooling loads in buildings [32]. These previous studies show SVR successfully has been employed in chilled water as well as heating and cooling load applications, but not to predict secondary flow rates in the DC substation. By predicting the secondary flow rates in DC supplied secondary systems the need to install temporary measurement equipment to obtain such data is diminished. However, steady state conditions rarely occur during normal operation and are difficult evaluate. SVR could therefore be a suitable method to predict secondary flow rates considering transient conditions and unsteady state.

1.2. Aim of study

Based on the review literature, there is a potential to improve the control of the secondary supply temperatures and limit the primary flow in buildings supplied by DC to increase the primary return temperature. This could be done by implementing new control strategies in the DC substation. For example, ensuring a sufficient temperature approach between the supply streams of the heat exchanger and testing a primary flow limiting control strategy. Neither of these control strategies have previously been practically evaluated in substations of a Swedish DC system. Moreover, unbalances between the primary and secondary flows of the HX cause inefficiencies, but the secondary flow rates are typically not measured nor have previously been investigated. The secondary flows could be roughly estimated by the HX heat balance to avoid installing flow measurement equipment but due to transient conditions and unsteady state another method is desirable.

The aim of this study is therefore threefold: 1) to investigate the effects on the primary return temperature by ensuring a 2 °C temperature approach between the supply streams; 2) to assess the practical outcomes of a flow limiting control strategy and evaluate its effects on the entire district cooling system; 3) to increase the knowledge about the secondary flows in DC substations by measurements, investigate potential unbalances of the primary and secondary flows and compare two different flow prediction methods.

2. District cooling system

The study is performed in the DC system in Gothenburg, Sweden, in cooperation with the utility provider with the aim to improve its performance. More information about the DC system can be found in Jangsten et al. [3,13] and local guidelines [15]. The DC system has been under development since 1990 and is being expanded to handle increased cooling loads in new buildings, in and around the city center.

2.1. DC substation control

The district cooling substation, shown in Fig. 1, is controlled according to the following [14,15,33]:

1. The building CHW system pump is demand controlled and starts by a time schedule or when there is a cooling demand in the building. The pump is typically a variable speed pump controlled by a differential pressure regulator in the system, although some systems have constant speed pumps operating on or off.
2. The setpoint of the CHW supply temperature is either set to a constant value, compensated based on the measured outdoor temperature or calculated using building parameters and weather data [13].
3. The setpoint is achieved by means of opening and closing the motorized control valve(s) which allows the primary water to flow through the heat exchanger. Larger substations have two control valves in parallel where the second control valve opens if the first one is open 100%.

In this paper, the following controlled entities of the district cooling substation will be focused on: 1) supply temperature on secondary side, 2) primary flow through the heat exchanger and 3) secondary flow through the heat exchanger. These three entities are interconnected and ultimately affect the temperature returned to the district cooling system.

The design guidelines of Swedish district cooling systems suggest a secondary supply temperature setpoint of 8 °C which should yield a secondary return temperature of 18 °C. This is based on primary supply and return temperatures being 6/16 °C, allowing for a 2 °C temperature approach between supply and return streams of the heat exchanger. The design guidelines also suggest equal flow rates for primary and secondary flows, with variations up to 10% higher flow rate for the secondary side compared to the primary if slightly different temperatures are chosen [14].

2.2. Operational data

The data in this paper are operational data obtained from substations in the district cooling system, see Table 1 and Fig. 1. The data have been collected from the energy meters used for billing purposes, owned by the utility company. Data have also been collected on the secondary side from the buildings' Supervisory Control and Data Acquisition (SCADA) systems. Secondary flow data was measured by complementary field measurement equipment as described in section 3.3.1.

The energy meter on the primary side is of the type Multical 801 [34] with temperature sensors of the type Thermowell RTD conforming to the standard EN 60751, class A, with an accuracy of ±0.2 °C [15]. The temperature sensors on the secondary side are also of the type Thermowell RTD and although not required to have an accuracy of ±0.2 °C, this is common practice. The data measured by the temperature sensors are recorded by two separate data collection systems, the primary side (for billing purposes by the
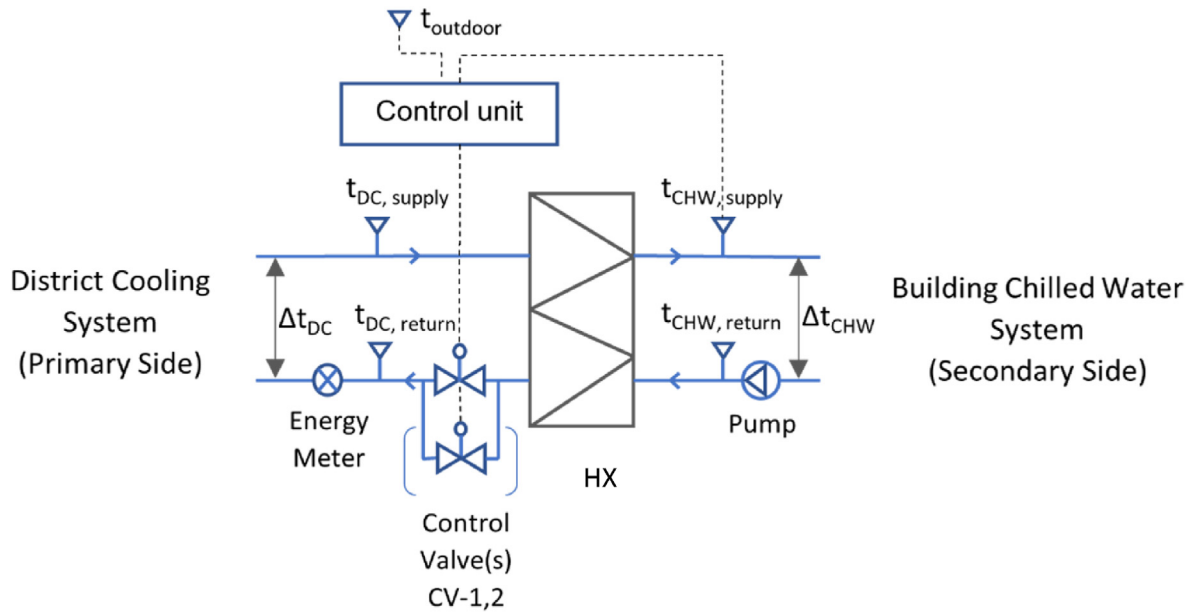
Fig. 1. Schematic of the district cooling substation with components, permanent measurement equipment and general control outline.

Table 1
Data used in the study, obtained from the substation energy meter, the buildings' SCADA systems and complementary field measurements.

Num-ber	Variable	Symbol	Unit	Type of data	Recording interval	Data collection system
1	DC-Power	$\dot{Q}_{DC}$	kW	Operational	1/h, hourly average	Energy meter
2	DC-Flow	$\dot{V}_{DC}$	m³/h	Operational	1/h, hourly average	Energy meter
3	DC-Supply Temperature	$t_{DC,supply}$	°C	Operational	1/h, instantaneous	Energy meter
4	DC-Return Temperature	$t_{DC,return}$	°C	Operational	1/h, instantaneous	Energy meter
5	DC-Delta-T	Δt_{DC}	°C	Calculated	1/h, instantaneous	
6	CHW-Supply Temperature	$t_{CHW,supply}$	°C	Operational	1/h, hourly average	Building SCADA system
7	CHW-Return Temperature	$t_{CHW,return}$	°C	Operational	1/h, hourly average	Building SCADA system
8	CHW-Delta-T	Δt_{CHW}	°C	Calculated	1/h, hourly average	
9	CHW-Flow	$\dot{V}_{CHW}$	m³/h	Complementary Measurement	1/10-min, instantaneous	Temporary field measurement equipment
10	DC-Supply Temperature	$t_{DC,supply.prod}$	°C	Operational	1/h, hourly average	DC operations management system
11	Outdoor Temperature	t_{out}	°C	Operational	1/h, hourly average	DC operations management system

utility company) and the secondary side (the SCADA system as owned by the building manager). The temperature sensors on the primary and secondary sides are not co-calibrated, and the measurements are also recorded with different intervals. The primary temperature sensors are instantaneous values, recorded once per hour whereas the secondary temperature measurements are hourly averages of more frequent readings during an hour.

The permanent flow meter accompanying the energy meter is of the type Ultraflow 54 with a tolerance of maximum 5% for the lowest flow of the dynamic range q_i:q_p according to standard EN 1434, where q_i is the lowest flow and q_p is the nominal flow [35]. For the substations in this study, q_i is 0.1–0.6 and q_p 10–60 m³/h. The primary flow is measured as the sum of flow during an hour. For the secondary flow rate measurements a portable ultrasonic clamp-on flow meter of the type TDS-100F from Ambiductor was used, similar to that in Ref. [9]. For installation, ten pipe diameters of unobstructed pipe length are required before the flow meter and five pipe diameters after. The secondary flow was measured instantaneously with a 10-min sampling frequency, calculated into hourly averages.

Despite differences in how the data are recorded, the preconditions of this study are the data available from the buildings' substations and SCADA systems. The point of departure of this

research is therefore the installed data collection systems and their obtainable data, however, recognizing the disparities and potential implications on the outcome.

2.3. Building information

The field tests were conducted in four different buildings with various business types: market hall and offices with restaurants and shops. In building 1 the CHW system serves the cooling coils of two AHUs, a chilled beam system and fan coil units which supply both space and process cooling demands. The CHW systems in buildings 2 and 3 each serve cooling coils of four AHUs and a chilled beam system. For all three buildings, the setpoints of the CHW supply temperature are determined from outdoor temperature compensated temperature curves. In building 4 the CWH system serves the cooling coils of seven AHUs, fan coil units and the condensers of refrigeration chillers. The cooling demand is a combination of space and process cooling. The CHW supply temperature setpoint is based on two different operation modes; cooling and heat recycling, which primarily depend on the outdoor temperature. When the operation is in cooling mode the setpoint is a constant value of 8 or 10 °C and shifted upwards when operating in heat recycling mode, recovering heat from the condensers.

3. Design of study

In section 3.1 and 3.2 the secondary supply temperature and primary flow limitations are described and in section 3.3 the secondary flow evaluations are found.

3.1. Secondary supply temperature minimum limitation

The secondary supply temperature minimum limitation was implemented by a control strategy limiting the setpoint of the secondary supply temperature to as a minimum be 2 °C higher than the current primary supply temperature, according to the design guidelines [15]. It was evaluated by a field test in buildings 1−3, by adding it to the existing control system of the buildings. The control strategy was programmed to read the $t_{DC, \, supply}$ and add a temperature difference of 2 °C to this value (see Fig. 1). This became the minimum limitation value for the $t_{CHW, \, supply}$ setpoint. If the $t_{CHW, \, supply}$ setpoint, as determined by the temperature curve for the present outdoor temperature, was lower than the current minimum limitation value, the $t_{CHW, \, supply}$ setpoint was set to the minimum limitation value. For building 1, the control strategy test period was from May 22nd until September 12th, 2021, with reference period being the same period the previous year. For buildings 2 and 3, the control strategy test period was from July 13th to September 15th and 9th, 2021, respectively, with reference period from May 3rd and May 22nd respectively to July 11th, 2021. Despite test and reference periods for the three buildings being different, the comparison with and without the control strategy was considered reasonable due to the occurrence of similar cooling demands and outdoor temperatures of the two periods. The goal of limiting the secondary supply temperature setpoint was to increase the primary return temperature and reduce the volume of primary district cooling water required per delivered MWh.

The setpoint limitation was also evaluated for building 1 in a heat exchanger simulation model called SSP G8. The simulation model is developed and used by SWEP International AB for designing, selecting, and evaluating the performance of heat exchangers [36]. The simulation was based on operational data from the period April−October 2020, extracted for weekdays between the hours 10:00−16:00 to increase the likelihood of having a stable cooling demand in the building.

3.2. Primary flow limitation

The primary flow limitation was assessed by field testing a control strategy limiting the flow through the HX to a fixed value, see section 3.2.1. The potential of this control strategy, if implemented in all substations of the DC system, is evaluated in section 3.2.2.

3.2.1. Field test

The flow limitation control strategy was programmed and added to the building's existing control system. It included a flow limit value and was set up to read the instantaneous water flow rate from the energy meter. When the water flow exceeds the flow limit value the control valve(s) start to close until the water flow is below the limit. The goal with the control strategy was to limit the flow to increase beyond the lowest flow for maximum cooling power, thereby avoiding operation in the saturation zone and increasing the primary delta-T. The flow limit value was therefore set to the lowest flow for maximum cooling power. The test period was from April 30th to September 14th, 2021, and the reference period was the same time period in 2020.

3.2.2. System benefits

The system benefit of a primary flow limitation was evaluated with hourly operational data from the period May−September 2018 from all 155 substations in the district cooling system. The data analyzed were variables 1−5 in Table 1. To determine the amount of flow in the saturation zone, the evaluation method for each substation was the following [3]:

1. Find the maximum cooling power.
2. Determine the lowest flow rate for maximum cooling power called "corresponding flow."
3. Sum hourly flows greater than the corresponding flow.

The result from each substation was inspected using correlation plots to identify outliers and erroneous data. Such substations were either removed from the analysis, or the data were corrected if possible.

3.3. Secondary flow evaluation

The secondary flow was measured in 16 substations, see section 3.3.1. Two models were created based on the measured data to predict the secondary flow when measurements are unavailable: 1) based on the heat balance of the HX, section 3.3.2 and 2) using support vector regression, section 3.3.3.

3.3.1. Field measurements

The flow measurements were carried out in periods of 2−3 weeks in two different buildings during the summer of 2019 and in 14 buildings during the summer of 2020. The buildings were selected based on feasibility of correct flow meter installation and availability of the property owners from previous collaborations (see Refs. [3,13]). Having secondary flow data, the effectiveness of the HX can be analyzed using the operational and measured data as input for the four temperatures and the two flow rates. The following equations have been used to evaluate the temperature effectiveness and NTU of the HX for each building where the secondary flow was measured [6,22,25]:

$$\eta = \frac{1 - e^{-NTU(1-R)}}{1 - R \cdot e^{-NTU(1-R)}} \tag{1}$$

where:

$$R = \frac{\dot{V}_{DC}}{\dot{V}_{CHW}} \tag{2}$$

$$NTU = \frac{\Delta t_{DC}}{LMTD} \tag{3}$$

$$LMTD = \frac{\Delta t_2 - \Delta t_1}{\ln \frac{\Delta t_2}{\Delta t_1}} \tag{4}$$

where $\Delta t_1 = t_{CHW,supply} - t_{DC,supply}$ [°C] and $\Delta t_2 = t_{CHW,return} - t_{DC,return}$ [°C] (see Fig. 1 for clarification), also called supply temperature approach and return temperature approach.

3.3.2. Heat balance model

A simple HX model can be created from the heat balance of the plate frame HX, assuming no phase change and constant specific heats of the two fluids. The heat transfer on the primary side of the HX is therefore equal to the heat transfer on the secondary side of the HX [25], as expressed by Eqn. (5):

$$\dot{Q}_{DC} = \dot{Q}_{CHW} \qquad (5)$$

Eqn. (5) can be expanded and rewritten as:

$$\dot{V}_{CHW} = \frac{\dot{V}_{DC} \cdot c_{p,w} \cdot \rho_w \cdot \left(t_{DC,return} - t_{DCsupply}\right)}{c_{p,w} \cdot \rho_w \cdot \left(t_{CHW,return} - t_{CHW,supply}\right)} \qquad (6)$$

where $\dot{V}_{DC}$ and $\dot{V}_{CHW}$ are the water flow rates on the primary and secondary sides of the HX, $t_{DC,return}$, $t_{DC,supply}$, $t_{CHW,return}$ and $t_{CHW,supply}$ are the inlet and outlet temperatures (see Table 1 for more information) and $c_{p,w}$ [kJ/(kg·°C)] and ρ_w [kg/m^3] are the specific heat capacity and density of water.

Eqn. (6) is valid when the system is in steady state. However, subject to the operational data of the investigated buildings in this paper, there is no simple method to determine when the buildings' CHW systems have reached steady state, if occurring at all for a sufficient amount of time. The secondary flow predictions are therefore based on operation which may be in both steady and unsteady state.

3.3.3. Support vector regression model

To compare the results of the heat balance model, a flow prediction model using support vector regression (SVR) was created. SVR is a machine learning algorithm based on structural risk minimization. If the data cannot be sufficiently described using linear regression it can be mapped to a high-dimensional feature space by the use of kernels. In this high-dimensional feature space, linear regression can be performed on the data to predict new values [29,37]:

$$y(x) = \sum_{i=1}^{N} (\alpha_i^* - \alpha_i) K(x_i, x) + b \qquad (7)$$

where $\alpha_i^* - \alpha_i$ are the coefficients of the support vectors, x_i is a vector from the training data set, $K(x_i, x)$ is a kernel function (see below for choice) and b is a coefficient determining the position of the separating hyperplane in the high-dimensional feature space. The SVR model was developed with MATLAB's regression learner application using the ε-insensitive loss function [37]. The variables of the train and test dataset can be found in Table 1, with $\dot{V}_{CHW}$ being the response variable and variables 2–8 being the predictor variables. Data from 10 different buildings were used to build the model.

Prior to building the SVR model the variables were evaluated for conformity to a normal distribution by calculating the skewness of each variable [38]:

$$s = \frac{E(X - \mu)^3}{\sigma^3} \qquad (8)$$

where E represents the expected value, X is a random variable, μ and σ it's mean and standard deviation. The criteria for conformity to a normal distribution was $-0.4 < s < 0.4$. Variables violating this criteria were transformed with Box-Cox transformation [39]:

$$y(\lambda) = \frac{y^\lambda - 1}{\lambda} \qquad (9)$$

where y is the data to be transformed and λ is the power transformation. After transformation, where applicable, all variables were normalized with z-score [40]:

$$Z = \frac{X - \mu}{\sigma} \qquad (10)$$

The dataset was split into a training and a testing dataset with 70% of the data used for training and 30% for testing. The available kernels within MATLAB's SVR application were each tested and the one yielding the highest R^2-value and lowest root-mean-square error (RMSE) was selected, which was the Gaussian kernel [41]:

$$K(x_i, x) = e^{-\gamma \|x_i - x\|^2} \qquad (11)$$

where γ is the width parameter of the kernel function.

The model training was done with cross-validation to protect against overfitting [42]. After training, the model was tested with the test dataset, which resulted in an RMSE of 0.266 and an R^2-value of 0.92. After testing, the model was used to predict the secondary flow for each of the 10 buildings separately. The prediction output was transformed back to the original scale of m^3/h using the mean and standard deviation of the normalized input vector and the λ-value from the Box-Cox transformation [43].

4. Results and discussion

4.1. Secondary supply temperature minimum limitation

The results from the field test of the setpoint minimum limitation control strategy showed it successfully limited the $t_{CHW,\,supply}$ setpoint to a minimum of $t_{DC,\,supply}$ +2 °C. In Fig. 2 the supply temperature approach of the HXs before and after implementation can be seen. The data analyzed have been extracted for weekdays between the hours 10−16 to eliminate potential temperature inaccuracies due to low or absent cooling needs. For buildings 1 and 3, the number of hours with a supply temperature approach lower than the limitation 2 °C were fewer with the control strategy compared to without. For building 2 there were no hours with a temperature approach <2 °C prior to installing the control strategy and its effect was therefore less noticeable. The supply temperature approaches have been calculated based on hourly average values of the secondary supply temperature, and instantaneous values for the primary supply temperature. The spread of the data points, along with temperature approaches <2 °C despite the setpoint limitation, are due to instantaneous temperatures from the primary side.

Fig. 2 and Table 2 show the primary return temperature and the supply temperature approach increased after the control strategy was implemented. However, this increase was not solely the result of implementing the setpoint limitation control strategy. During the summer of 2021, new secondary supply temperature setpoint curves were also tested and implemented by the building owner in all three buildings, contributing to the increased temperatures. For building 1, the temperature increases with the control strategy for the old and the new temperature curves were evaluated separately, see Table 2. It is evident the control strategy and the new temperature curve resulted in a higher primary return temperature, +2.3 °C, compared with the control strategy and the old temperature curve, +1.0 °C. It is therefore important to optimize the supply temperature curve of the building to achieve the highest possible primary return temperature. In Table 2, the results from the simulation in the heat exchanger model for building 1 can also be found. The increase in primary return temperature was lower than in the field test, 0.3 °C compared to 1.0 °C.

Since the temperatures are obtained from two different systems and recorded differently, the calculations of the HXs' temperature approaches are less accurate than the values reported. The
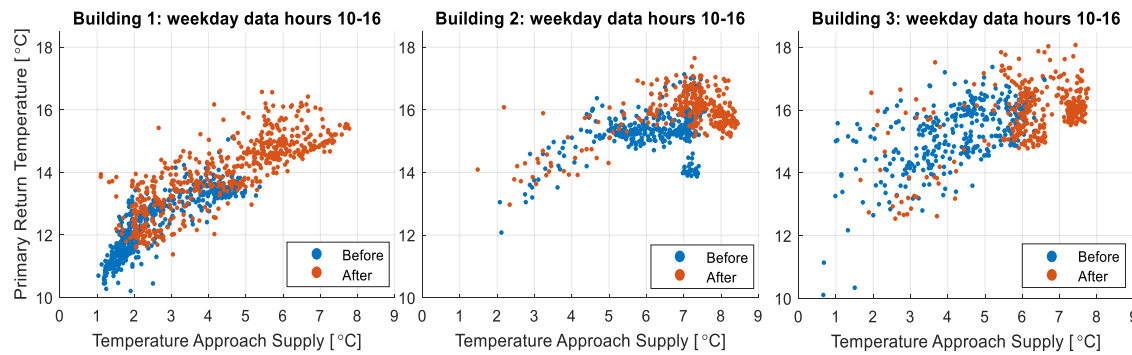
Fig. 2. Supply temperature approaches vs. primary return temperatures for buildings 1–3. For building 1 the setpoint limitation control strategy was tested May−September 2021 ("after"), with May−September 2020 as reference ("before"). For buildings 2 and 3, the control strategy was tested mid-July to mid-September of 2021 ("after") with May to mid-July 2021 as reference ("before").

Table 2
Mean difference of primary return temperature, secondary supply temperature and volume of primary side district cooling water per delivered MWh with the control strategy.

Building number	Dataset	Difference primary return temperature[a] [°C]	Difference secondary supply temperature[a] [°C]	Difference primary volume per delivered MWh[a] [m³/MWh]
1	Entire period	+1.6	+1.6	−33.7
	Old temperature curve	+1.0	+0.7	−21.6
	New temperature curve	+2.3	+2.6	−38.2
	Simulation in HX model	+0.3	+0.2	NA
2	Entire period	+0.6	+1.0	−5.1
3	Entire period	+0.7	+2.2	−16.5

[a] Mean values, difference between test and reference period.

temperature approaches are reported to 0.1 °C; however, the measurement uncertainties could be larger than tenth of a degree. The absolute temperatures of the temperature approaches are therefore only accurate to whole degrees.

The control strategy was more effective in building 1 compared to buildings 2 and 3. A potential reason is the greater need of such a control strategy due to low primary return temperatures and supply temperature approaches <2 °C. Regardless, the setpoint limitation had a positive impact in all three buildings. It was also evident optimizing the outdoor temperature compensated temperature curves is more important than installing the setpoint limitation to achieve higher primary return temperatures. Yet, the setpoint limitation is useful to always ensure a sufficient temperature approach and to avoid low primary return temperatures regardless of operating condition.

4.2. Primary flow limitations

This section comprises the results from the field test of the flow limitation control strategy and its potential on the entire district cooling system.

4.2.1. Evaluation of field test

In this section, the results from implementing the flow limitation control strategy to the control system of building 4 are presented. The response time of the control strategy was analyzed with two days of 10-min time resolution data. The flow limitation effectively reduced the flow from a limit violation around 5 m³/h to a flow below the limit within 10 min. The remaining data had an hourly time resolution, whereby the instantaneous flow may have been higher than the flow limit although not disclosed by the hourly data.

In Fig. 3, the cooling power and primary delta-T are shown as a function of primary flow for the reference period (without flow limitation) and for the test period (with flow limitation), extracted for operation in cooling mode. The limit was set to 25 m³/h, considered to be the corresponding lowest flow for the maximum cooling power based on data from 2020 (see Fig. 3 left). During the test period, the flow limitation came into effect during at least nine days. The control strategy was able to successfully restrict the primary flow to remain below the limit and completely eliminate flow in the saturation zone. This can be seen when comparing the left and the right graphs of Fig. 3. During the test period, the maximum flow was halved and the primary delta-T increased. Using data from Fig. 3, the median primary delta-T for flow rates >20 m³/h increased from 5.3 °C to 6.5 °C. Moreover, the total volume during the test period was reduced with 44% compared to the reference period. However, during 2021, the setpoint on the secondary side was changed by the building owner from previously being fixed at 8 °C for outdoor temperatures >15 °C, to be fixed at 10 °C for the same outdoor temperatures. In addition to the flow limitation, this was a major contributing factor for the large differences in primary flow between the two periods.

To evaluate the effects of different setpoints and flow limit values, the operating condition for most of the summer (test case 1) was compared with three other test cases (for example changing the secondary supply temperature setpoint back to 8 °C), conducted for different time periods, see Table 3.

The results from each test case in Table 3 have been compiled for hours when the flow limitation actively reduced the flow during operation in cooling mode. The primary return temperature was the highest for a flow limit of 25 m³/h and a setpoint of 10 °C and lowest for a flow limit of 25 m³/h with setpoint 8 °C. For a flow limitation of 17 m³/h the primary and secondary return
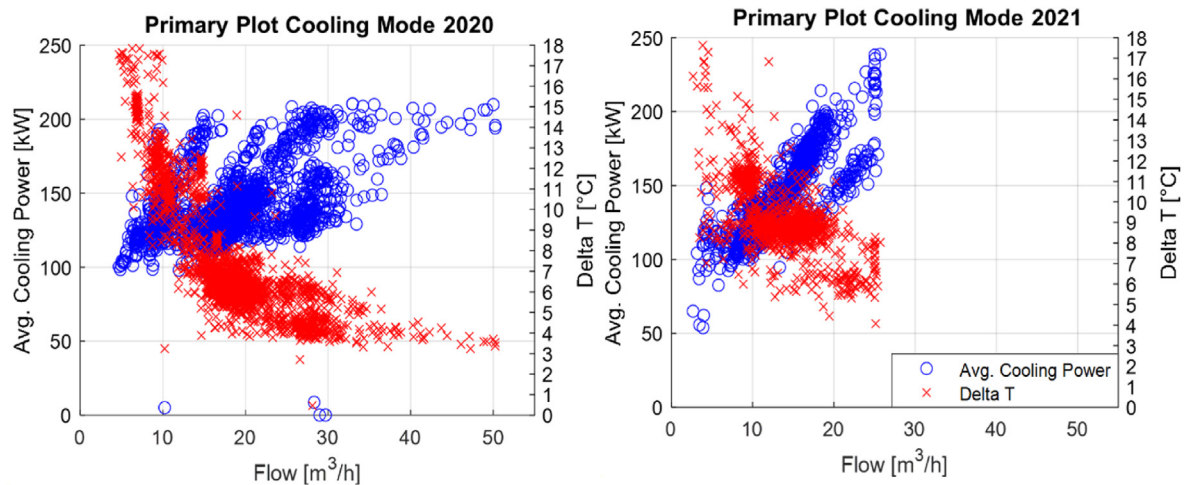
Fig. 3. Primary data as obtained from the energy meter for operation in cooling mode. Left: reference period without the flow limitation control strategy. Right: test period with the control strategy.

Table 3
Test cases and results of different flow limits and secondary setpoint combinations.

Test cases	1	2	3	4
Flow limitation [m³/h]	25	25	20	17
Secondary supply setpoint [°C]	10	8	8	8
Data resolution and time period	Hourly, entire test period	Hourly, 3 days	10-min, 1 day	10-min, 1 day
Results, median values				
Primary Return Temperature [°C]	15.8	12.8	14.3	15.3
Secondary Supply Temperature [°C]	10.5	8.0	8.2	8.8
Secondary Return Temperature [°C]	19.1	16.1	19.1	19.3

temperatures were also high, 15.3 and 19.3 °C respectively, despite the secondary setpoint of 8 °C not being reached. Since the primary return temperatures are instantaneous values and the secondary temperatures are hourly average values, their comparison is only approximate.

4.2.2. Flow in saturation zone for all substations

The hourly flow in the saturation zone for all substations in the DC system is shown in Fig. 4 for the period of April–October 2018. The total volume of flow in the saturation zone is equal to $103 \cdot 10^3$ m³, corresponding to 1.1% of the total DC system volume during this period. The highest hourly saturation zone flow was 546 m³/h and occurred on July 31st. Compared to the total flow rate in the DC system for that hour it corresponds to 8.4%.

According to Fig. 4, three peaks with a substantial saturation zone flow, >400 m³/h, occurred on May 8th, July 16th, and July 31st. During these days the DC supply temperature was greater than the 6 ± 1 °C design temperature, instead up to 10 °C. However, it can also be seen the supply temperature has been significantly higher than 6 ± 1 °C on other days without causing a substantial flow in the saturation zone. Another contributing factor to flow in the saturation zone is the outdoor temperature, affecting the actual cooling demands. It is evident a considerable amount of chilled water can be saved if each substation avoids flow in the saturation zone. An excessively high primary supply temperature is one reason to flow in the saturation zone. The secondary supply setpoint limitation control strategy can ensure a sufficient temperature approach if the primary supply temperature increases, thereby avoiding flow in the saturation zone with the primary flow limitation control strategy as back-up.

4.3. Secondary flow evaluation

In part one of this section the results from the field measurements of the secondary flow rates are presented and in part two the predictions of the secondary flow rates.

4.3.1. Flow measurements

The results from the field measurements of the secondary flow in the substation is presented along with a temperature effectiveness-NTU analysis. As recommended in the design guidelines for DC substations, the flow rates on the primary and secondary sides of the HX should be balanced [14]. However, as shown in Fig. 5, reality may deviate from design. In the left graphs the measured secondary flow is higher than the primary flow for building 2, and for building 5 the results are the opposite. Out of 16 buildings, balanced primary and secondary flow rates were only found in two. In the right graphs the HX temperature effectiveness (Eqn. (1)) as a function of NTU (Eqn. (3)) can be seen to decrease for an increased R (flow rate ratio between primary and secondary flows, Eqn. (2)). The design temperature effectiveness is 0.83, and for building 2 it is ≥ 0.83 for almost all hours. Conversely for building 5, a temperature effectiveness ≥ 0.83 is only achieved with $R \leq 1$ and a sufficiently large NTU. Similar trends could be observed for the remaining 14 buildings, where the design temperature effectiveness only could be reached with an $R \leq 1$, in agreement with [6,22].

The dynamic range, $q_i : q_p$ for the permanent flow meters in buildings 2 and 5 are 0.4−40 and 0.10−10 m³/h respectively. As shown in the left graphs of Fig. 5, the primary flow is within this range for building 2. However, for building 5 both upper and lower
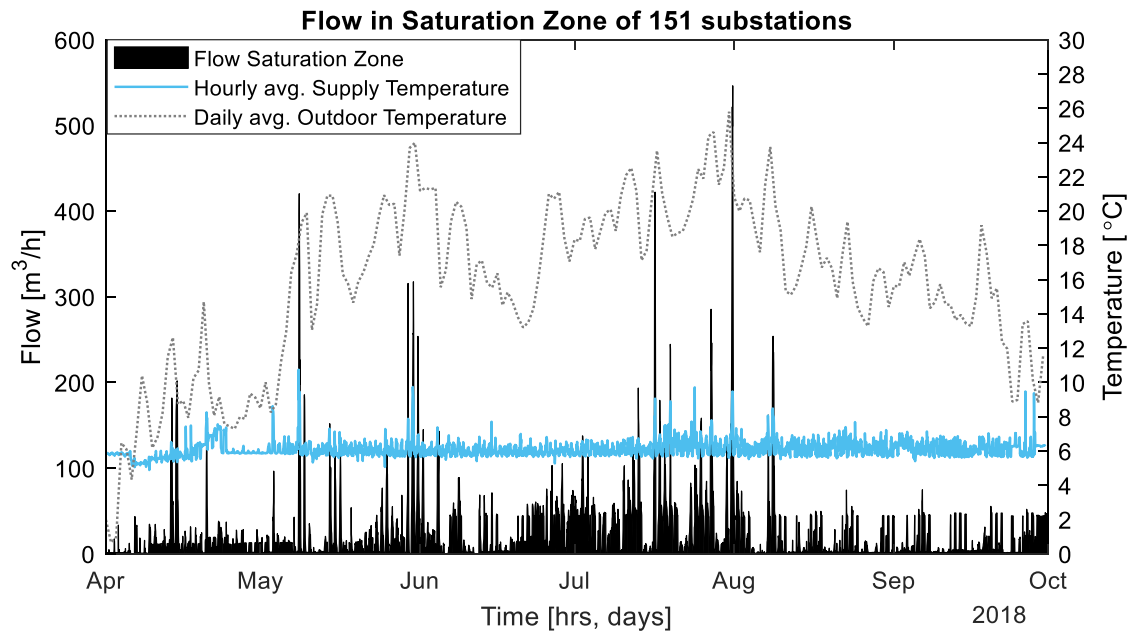
Fig. 4. Flow in the saturation zone of 151 substations, daily average outdoor temperature and hourly average supply temperature from the production plant, from April to October of 2018.
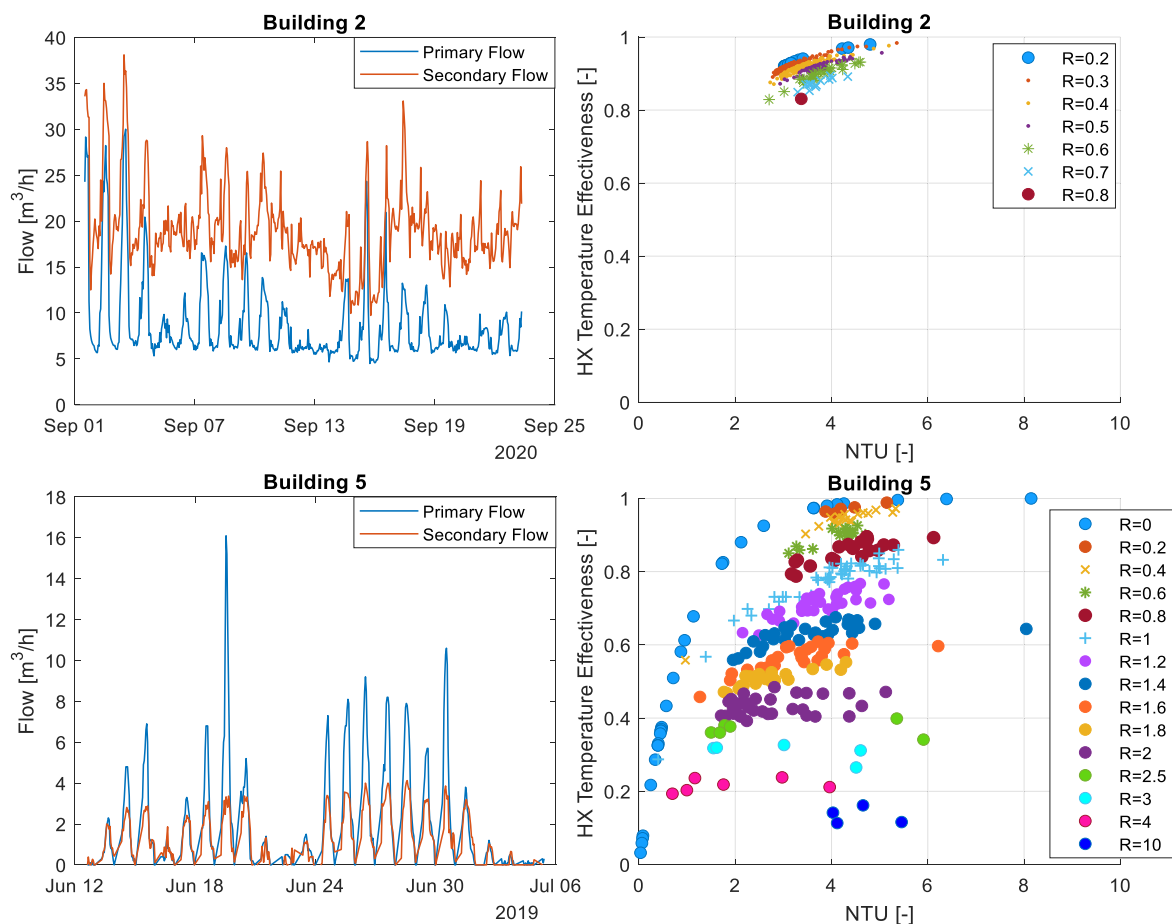

Fig. 5. Left: primary flow rates as measured by the permanently installed flow meter and secondary flow rates from field measurements for buildings 2 and 5. Right: Analysis of heat exchanger temperature effectiveness as a function of NTU and flow rate ratio R for buildings 2 and 5.

limits of the dynamic range are exceeded, and such data may be less accurate than data within the range. The installation of the clamp-on flow meter was conducted according to the installation manual. Parameters such as signal strength and measured versus calculated time for the ultrasound beam were within recommended limits. It should be noted the primary flow is the sum of flow during an hour, while the secondary flow is instantaneous measurements every 10-min, converted into hourly averages.

4.3.2. Flow predictions

In Fig. 6, the results of the predicted secondary flow based on the heat balance model and the SVR model are shown. The R^2 and RMSE values of fitting a linear model to the predictions by the SVR model was 0.89 and 4.19. For the heat balance model, R^2 was 0.79 and RMSE 7.32. This shows the SVR model was able to predict the secondary flow rate to a higher accuracy than the HX heat balance model. A potential a reason could be the operational data being input to both models. The heat balance model assumes steady-state and the SVR model can capture some of the non-linearity occurring during dynamic operating conditions. Moreover, the operational data were obtained from three different data collection systems (energy meter for billing purposes, building SCADA system and field measurements with temporary equipment). Each of these measurements has its own uncertainty along with potential differences from for example the timestamps, possibly off-setting the hourly data from each system.

The fitted lines for the SVR and the heat balance models in Fig. 6 are both based on minimizing the sum of squares due to error. For this reason, they deviate from the "theoretical fit", dependent on the fact that the measured secondary flow should be equal to the predicted secondary flow. It shows the heat balance model predicts higher secondary flows whereas the SVR model predicts slightly lower secondary flows.

4.4. Reflections

The fact that this study is based on measurements from different systems with different time resolution and accuracies makes the evaluation somewhat cumbersome. Regardless, the results prove the implemented control strategies are valuable both in existing substations and in the design of new, to improve the overall performance of the DC system.

Existing guidelines regulate the design of the DC substations [14,15,33]. However, as shown in this study and preceding study [3], reality deviates from design. Four main reasons can be identified: 1) the early development of the DC system connected buildings with existing cooling systems with traditional chillers, 2) the DC substations are designed by different consultants on behalf of the building owners, 3) building cooling load estimations are oftentimes inaccurate and lead to oversizing, and 4) the DC design guidelines have only been applied since 2012.

5. Conclusions

In this article, three aspects of the district cooling substation design and control were investigated with the goal to increase the primary return temperature. The three aspects involved 1) the secondary supply temperature setpoint, 2) the primary flow rate and 3) the flow rate relation between the primary and secondary flows. For aspect one, a setpoint limitation control strategy was evaluated by field tests in three buildings resulting in an increased primary return temperature of 0.6−1.6 °C. For aspect two, a flow limitation control strategy was field tested in one building. The test resulted in an increased primary return temperature with 1.2 °C and elimination of flow in the saturation zone. If the flow limitation control strategy was implemented in all substations, a collective saturation zone equal to 1.1% of the total DC system volume during April−October could be avoided. For aspect three, field measurements revealed higher primary flow rates than secondary in some substations and lower in other. However, the NTU-effectiveness analysis showed the primary flow rate has to be balanced with or lower than the secondary flow rate to achieve design temperature effectiveness of the heat exchanger. Since measured secondary flow rates normally cannot be obtained, a support vector regression and a heat balance model were developed to predict the secondary flow rates. It was shown the support vector regression model achieved a higher accuracy owing to potential transient conditions. The results of this study indicate all three investigated aspects of the substation design and control affect the ability to achieve high primary return temperatures. The tested control strategies can facilitate higher primary return temperatures and evaluating the flow rate relation could identify further potentials of increased primary return temperatures. By conducting field tests and measurements in real buildings, this study contributes with an understanding of the actual operation of district cooling substations. Moreover, it indicates how the systems on either side of the heat exchanger respond when implementing the investigated control strategies. This knowledge could support the utility company to encourage other building owners to implement the same control strategies, ultimately increasing the primary return temperature in the entire district cooling system.

Credit author statement

Maria Jangsten: Conceptualization, Methodology, Investigation, Writing - Original Draft. **Torbjörn Lindholm:** Writing - Review & Editing, Supervision. **Jan-Olof Dalenbäck:** Writing - Review & Editing, Supervision, Funding acquisition.

Declaration of competing interest

The authors declare that they have no known competing financial interests or personal relationships that could have appeared to influence the work reported in this paper.
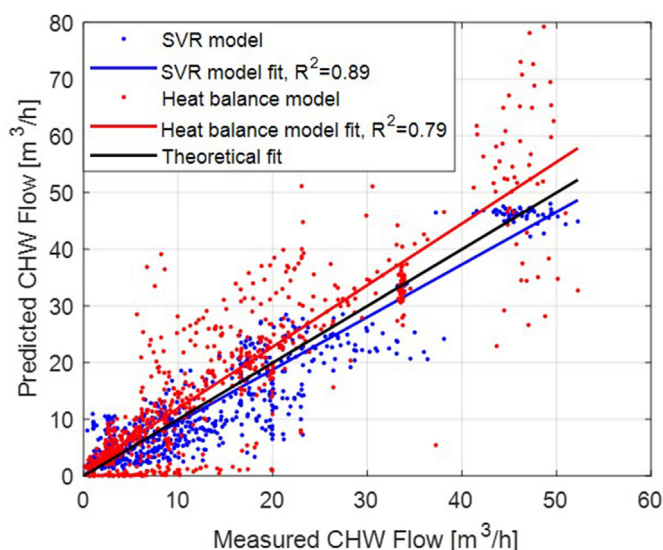

Fig. 6. Predicted secondary flow with heat balance and support vector regression model vs. measured secondary flow.

Acknowledgements

References

[1] IEA. The Future of Cooling: opportunities for energy-efficient air conditioning. Paris. 2018. https://doi.org/10.1787/9789264301993-en.

[2] Moe EM. Building performance with district cooling. ASHRAE J 2005;47: 46–53.

[3] Jangsten M, Lindholm T, Dalenbäck JO. Analysis of operational data from a district cooling system and its connected buildings. Energy 2020;203. https://doi.org/10.1016/j.energy.2020.117844.

[4] Ntakolia C, Anagnostis A, Moustakidis S, Karcanias N. Machine learning applied on the district heating and cooling sector: a review. Energy Systems 2021. https://doi.org/10.1007/s12667-020-00405-9.

[5] Buffa S, Fouladfar Hossein M, Franchini G, Gabarre Lozano I, Chicote MA. Advanced control and fault detection strategies for district heating and cooling systems—a review. Appl Sci 2021;11:1–32. https://doi.org/10.3390/app11010455.

[6] Frederiksen S, Werner S. District heating and cooling. Studentlitteratur AB; 2014.

[7] Gao D, Wang S, Sun Y, Xiao F. Diagnosis of the low temperature difference syndrome in the chilled water system of a super high-rise building: a case study. Appl Energy 2012;98:597–606. https://doi.org/10.1016/j.apenergy.2012.03.057.

[8] Ljunggren P, Johansson P-O, Wollerstrand J. Optimised space heating system operation with the aim of lowering the primary return temperature. In: The 11th international symposium on district heating and cooling; 2008.

[9] Lauenburg P, Wollerstrand J. Adaptive control of radiator systems for a lowest possible district heating return temperature. Energy Build 2014;72:132–40. https://doi.org/10.1016/j.enbuild.2013.12.011.

[10] Gustafsson J, Delsing J, van Deventer J. Improved district heating substation efficiency with a new control strategy. Appl Energy 2010;87:1996–2004. https://doi.org/10.1016/j.apenergy.2009.12.015.

[11] Gustafsson J, Delsing J, van Deventer J. Experimental evaluation of radiator control based on primary supply temperature for district heating substations. Appl Energy 2011;88:4945–51. https://doi.org/10.1016/j.apenergy.2011.06.050.

[12] Oevelen T Van, Vanhoudt D, Salenbien R. Evaluation of the return temperature reduction potential of optimized substation control. Energy Proc 2018;149: 206–15. https://doi.org/10.1016/j.egypro.2018.08.185.

[13] Jangsten M, Filipsson P, Lindholm T, Dalenbäck J-O. High temperature district cooling: challenges and possibilities based on an existing district cooling system and its connected buildings. Energy 2020;199:117407. https://doi.org/10.1016/j.energy.2020.117407.

[14] Sverige Energiföretagen. Fjärrkylcentralen - utförande och installation. 2019.

[15] Göteborg Energi AB. Lokala anvisningar för fjärrkyla. 2021.

[16] Gao D ce, Wang S, Shan K. In-situ implementation and evaluation of an online robust pump speed control strategy for avoiding low delta-T syndrome in complex chilled water systems of high-rise buildings. Appl Energy 2016;171: 541–54. https://doi.org/10.1016/j.apenergy.2016.03.077.

[17] Guelpa E, Marincioni L. Demand side management in district heating systems by innovative control. Energy 2019;188. https://doi.org/10.1016/j.energy.2019.116037.

[18] Thuillard M, Reider F, Henze GP. Energy efficiency strategies for hydronic systems through intelligent actuators. ASHRAE J 2014;1–8.

[19] Kuosa M, Aalto M, El Haj Assad M, Mäkilä T, Lampinen M, Lahdelma R. Study of a district heating system with the ring network technology and plate heat exchangers in a consumer substation. Energy Build 2014;80:276–89. https://doi.org/10.1016/j.enbuild.2014.05.016.

[20] Laajalehto T, Kuosa M, Mäkilä T, Lampinen M, Lahdelma R. Energy efficiency improvements utilising mass flow control and a ring topology in a district heating network. Appl Therm Eng 2014;69:86–95. https://doi.org/10.1016/j.applthermaleng.2014.04.041.

[21] Iturralde J, Kuosa M, Mäkilä T, Lampinen M, Lahdelma R. Heat exchanger measurements in a mass flow controlled consumer substation connected to a ring network. Appl Therm Eng 2015;90:733–41. https://doi.org/10.1016/j.applthermaleng.2015.07.005.

[22] Kandlikar SG, Shah RK. Multipass plate heat exchangers-effectiveness-NTU results and guidelines for selecting pass arrangements. J Heat Tran 1989;111:300–13. https://doi.org/10.1115/1.3250678.

[23] Zaleski T, Klepacka K. Plate heat exchangers-method of calculation, charts and guidelines for selecting plate heat exchanger configurations. Chem Eng Process 1992;31:49–56. https://doi.org/10.1016/0255-2701(92)80008-Q.

[24] Gut JAW, Pinto JM. Modeling of plate heat exchangers with generalized configurations. Int J Heat Mass Tran 2003;46:2571–85. https://doi.org/10.1016/S0017-9310(03)00040-1.

[25] Incropera FP, Dewitt DP, Bergman TL, Lavine AS. Fundamentals of heat and mass transfer. sixth ed. John Wiley & Sons, Inc.; 2007.

[26] Gao D, Wang S, Shan K, Yan C. A system-level fault detection and diagnosis method for low delta-T syndrome in the complex HVAC systems. Appl Energy 2016;164:1028–38. https://doi.org/10.1016/j.apenergy.2015.02.025.

[27] Al-Dawery SK, Alrahawi AM, Al-Zobai KM. Dynamic modeling and control of plate heat exchanger. Int J Heat Mass Tran 2012;55:6873–80. https://doi.org/10.1016/j.ijheatmasstransfer.2012.06.094.

[28] Gao DC, Wang S, Gang W, Xiao F. A model-based adaptive method for evaluating the energy impact of low delta-T syndrome in complex HVAC systems using support vector regression. Build Serv Eng Technol 2016;37:576–96. https://doi.org/10.1177/0143624416640760.

[29] Vapnik VN. The nature of statistical learning theory. second ed. 2000. https://doi.org/10.1007/978-1-4757-3264-1.

[30] Zhao Y, Wang S, Xiao F. A system-level incipient fault-detection method for HVAC systems. HVAC R Res 2013;19:593–601. https://doi.org/10.1080/10789669.2013.789371.

[31] Liu Y, Hu X, Luo X, Zhou Y, Wang D, Farah S. Identifying the most significant input parameters for predicting district heating load using an association rule algorithm. J Clean Prod 2020;275. https://doi.org/10.1016/j.jclepro.2020.122984.

[32] Li X, Yao R. A machine-learning-based approach to predict residential annual space heating and cooling loads considering occupant behaviour. Energy 2020;212:118676. https://doi.org/10.1016/j.energy.2020.118676.

[33] Göteborg Energi AB. Handbok för effektiv fjärrkyladrift. 2016.

[34] Kamstrup A/S. Technical description multical 801. 2015.

[35] Kamstrup A/S. Technical description Ultraflow 54. 2015.

[36] SWEP International AB. SSP G8 Info package. 2019.

[37] The MathWorks Inc. Understanding support vector machine regression. n.d. https://se.mathworks.com/help/stats/understanding-support-vector-machine-regression.html. [Accessed 19 October 2021].

[38] Pham H. Springer handbook of engineering statistics, vol. 91; 2017.

[39] Box GEP, Cox DR. An analysis of transformations. Journal, Source Statistical, Royal Series, Society 1964;26:211–52.

[40] Bonamente M. Statistics and analysis of scientific data. second ed. Springer; 2017.

[41] Chang C-C, Lin C-J. LIBSVM: a Library for support vector machines. ACM Transactions on Intelligent Systems and Technology 2011;2. https://doi.org/10.1145/1961189.1961199.

[42] The MathWorks Inc. Train regression models in regression learner app. n.d. https://se.mathworks.com/help/stats/train-regression-models-in-regression-learner-app.html. [Accessed 19 November 2021].

[43] Cox DR. Nonlinear models, residuals and transformations 1. Series Statistics 1977;8:3–22. https://doi.org/10.1080/02331887708801354.